

CriSp: Leveraging Tread Depth Maps for Enhanced Crime-Scene Shoeprint Matching

Samia Shafique¹ Shu Kong² Charless Fowlkes¹
¹University of California, Irvine ³Texas A&M University
sshafiqu@uci.edu shu@tamu.edu fowlkes@ics.uci.edu
<https://github.com/Samia067/CriSp>

Abstract. Shoeprints are a common type of evidence found at crime scenes and are used regularly in forensic investigations. However, existing methods cannot effectively employ deep learning techniques to match noisy and occluded crime-scene shoeprints to a shoe database due to a lack of training data. Moreover, all existing methods match crime-scene shoeprints to clean reference prints, yet our analysis shows matching to more informative tread depth maps yields better retrieval results. The matching task is further complicated by the necessity to identify similarities only in corresponding regions (heels, toes, etc) of prints and shoe treads. To overcome these challenges, we leverage shoe tread images from online retailers and utilize an off-the-shelf predictor to estimate depth maps and clean prints. Our method, named *CriSp*, matches crime-scene shoeprints to tread depth maps by training on this data. *CriSp* incorporates data augmentation to simulate crime-scene shoeprints, an encoder to learn spatially-aware features, and a masking module to ensure only visible regions of crime-scene prints affect retrieval results. To validate our approach, we introduce two validation sets by reprocessing existing datasets of crime-scene shoeprints and establish a benchmarking protocol for comparison. On this benchmark, *CriSp* significantly outperforms state-of-the-art methods in both automated shoeprint matching and image retrieval tailored to this task.

Keywords: shoeprint matching · image retrieval · forensics

1 Introduction

Examining the evidence found at a crime scene assists investigators in identifying perpetrators. Shoeprints are more likely to be found at crime scenes, though they may possess fewer distinct identifying features compared to other biometric samples like blood or hair [11]. Consequently, analyzing shoeprints can furnish crucial leads to aid investigators in narrowing down potential suspects in a crime.

The examination of shoeprints forensically offers insights into both the class attributes and the acquired attributes of the perpetrator’s footwear. Class attributes pertain to the general features of the shoe, such as its brand, model, and size. On the other hand, acquired attributes encompass the unique traits that develop on a shoe with wear and tear, such as holes, cuts, and scratches. Our focus lies in facilitating the investigation of the class attributes of shoeprints.

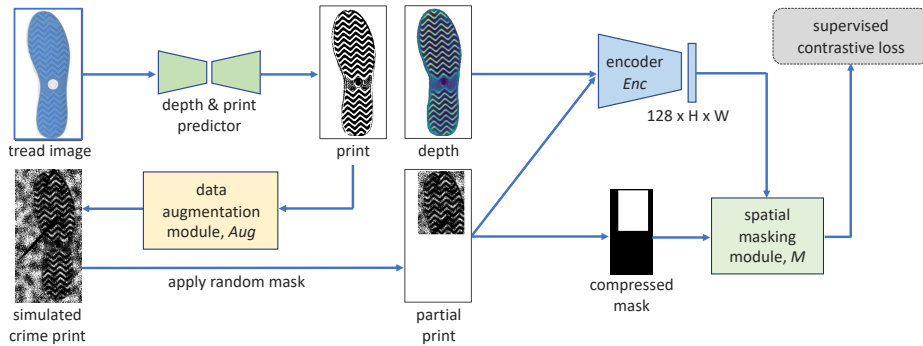


Fig. 1: We develop a method termed *CriSp* to compare crime-scene shoeprints against a database of tread depth maps (predicted from tread images collected by online retailers) and retrieve a ranked list of matches. We train *CriSp* using tread depth maps and clean prints (Sec. 4) as shown above. We use a data augmentation module *Aug* to address the domain gap between clean and crime-scene prints, and a spatial feature masking strategy (via spatial encoder *Enc* and masking module *M*) to match shoeprint patterns to corresponding locations on tread depth maps (Sec. 5). *CriSp* achieves significantly better retrieval results than the prior methods (Sec. 6)

Status quo. Traditional automated shoeprint matching methods [3–5, 12, 16, 22, 27, 28, 50] typically use handcrafted priors to match crime-scene shoeprints with clean, reference impressions. Recent approaches [26, 33, 53] propose using more generalizable features from Convolutional Neural Networks (CNNs), yet they are limited to using CNNs pretrained on ImageNet [17] since available datasets [29] are small and not suitable for training. Training on shoeprint-specific data is expected to improve matching performance. Importantly, while existing methods match crime-scene shoeprints to clean reference shoeprints, our findings suggest that matching to tread depth maps containing 3D shape information is more effective (see details in Sec. 6.3).

Motivation. To address the need for a large-scale training dataset, our proposal leverages the extensive collection of tread images of various shoe products available from online retailers. Tread depth maps and clearly visible prints can be predicted from these images using [43]. Example tread images and their depth and print predictions are illustrated in Fig. 3. It is important to note that matching directly to RGB tread images causes models to overfit to irrelevant details such as albedo and lighting (see Sec. 6.3). *We formulate our problem as the retrieval of tread depth maps that best match crime-scene shoeprints by learning a representation from tread depth maps and clean shoeprints.*

Technical insights. We develop a method termed *CriSp* to address this problem using 3 key components (Fig. 1). Firstly, we employ a data augmentation module *Aug* to generate simulated crime-scene shoeprints from the clearly visible prints used during training. In an ideal scenario, learning a feature representation to match crime-scene shoeprint images to tread depth maps would require a dataset containing paired crime-scene shoeprints and corresponding tread depth

maps. In the absence of such data, our data augmentation module in combination with our training set of paired tread depth maps and clean prints serves as a viable alternative. Secondly, we propose a spatial encoder Enc to ensure that our model learns to match patterns in corresponding regions of shoe treads. For instance, if a crime-scene shoeprint exhibits stripes on the heels, the model must retrieve shoes with stripes in the heel region rather than other areas like the toe region. Thirdly, we incorporate a feature masking module M to ensure that only the visible portions of shoeprints affect our retrieval results when crime-scene shoeprints are only partially visible. We observe that combining these three techniques facilitates effective feature learning and results in significantly improved retrieval performance compared to existing state-of-the-art methods.

Contributions. Our paper makes three major contributions.

- We introduce the concept of matching crime-scene shoeprints to tread depth maps, leading to improved retrieval performance compared to traditional shoeprint matching methods.
- We propose a benchmarking protocol to evaluate our method against state-of-the-art approaches. This involves the creation of a new dataset, reprocessing of existing datasets, and defining appropriate evaluation metrics.
- We develop a spatially-aware matching method named *CriSp*, which demonstrates superior performance over existing methods in both shoeprint matching and image retrieval tailored to this specific task.

2 Related Work

Automated shoeprint matching. The success of automated fingerprint identification systems [15] has inspired researchers to study automated shoeprint matching. Current literature aims to extract features from crime-scene shoeprints and match them to a database of laboratory footwear impressions to identify the shoe make and model [41]. Holistic methods process the shoeprint image as a whole. Examples of this method use Hu’s moment [3], Zernike moment [50], and Gabor and Zernike features [27]. In contrast, local methods extract discriminative features from local regions of the shoeprint, making them more adept at handling partial prints. For instance, [28] exploit Wavelet-Fourier transform features, [4] introduce a block sparse representation technique, and [5] combine the Harris and the Hessian point of interest detectors with SIFT descriptors. Recent works [26, 33, 53] propose using features from networks pretrained on ImageNet [17] for their generalizability. However, the lack of large-scale shoeprint datasets hampers their effectiveness. To address this, we propose creating a large-scale training dataset by leveraging tread images from online retailers and utilizing an off-the-shelf predictor [43] to estimate their depth and print. This approach enables learning features from informative tread depth maps rather than shoeprints, ensuring good performance even with partially visible prints.

Image retrieval. Image retrieval techniques have been a popular research problem for several decades [54]. Traditional methods use handcrafted local features [9, 32], often coupled with approximate nearest-neighbor search methods

using KD trees or vocabulary trees [10, 23, 34, 37]. More recently, the success of CNNs in classification tasks [30] encouraged their use in image retrieval tasks [8, 44]. Global features can be generated by aggregating CNN features [6, 7, 21, 35, 39, 40, 48, 49, 51], while local features can also be used for spatial verification [13, 25, 35, 37, 51] which ensure better performance by using geometric information of objects. Our problem differs from this category of work since our query and database data come from different domains - crime-scene shoeprints and depth maps of shoe treads. Even within our query set of crime-scene shoeprints, images can be from various sources such as blood, dust, and sand impressions.

Cross-domain image retrieval. More closely related to our work is cross-domain image retrieval (CDIR), where the query and database images come from different domains. The fundamental idea is to map both domains into a shared semantic feature space to alleviate the cross-domain gap. Learning a distinct representation for each shoe model can be categorized as fine-grained cross-domain image retrieval (FG-CDIR) as we aim to retrieve one instance from a gallery of same-category images. It is harder than category-level classification [18, 19, 52] tasks since the differences between shoe treads are often subtle. A popular problem of this category, fine-grained sketch-based image retrieval (FG-SBIR), was introduced as a deep triplet-ranking based siamese network [38] for learning a joint sketch-photo manifold. FG-SBIR was improvised via attention-based modules with a higher order retrieval loss [46], textual tags [14, 45], and hybrid cross-domain generation [36]. Recently, [42] leveraged a foundation model (CLIP) and [31] explicitly learned local visual correspondence between sketch and photo to offer explainability. These works differ from ours in that we do not have any ground-truth training data from our query domain, and thus have to simulate it as best as we can. Additionally, our aligned query and database images enable us to use spatially-aware techniques like spatial feature masking.

3 Problem Setup and Evaluation Protocol

Our goal is to retrieve shoe models that best match crime-scene impressions by comparing against a comprehensive shoe collection. We propose using tread images from online retailers to build our reference database. The problem formulation and evaluation protocol is outlined below.

3.1 Problem setup

Tread depth maps are more informative and relevant than RGB tread images (refer to Sec. 6.3). Since there is no dataset of crime-scene shoeprints with ground-truth tread depth maps, we propose to learn from tread depth maps and clean shoeprints predicted from RGB tread images (details in Sec. 4.1) instead. A crime-scene investigator may want to use our method to get a ranked list of shoe models that match a crime-scene shoeprint and opt to manually inspect them. Therefore, **the problem is to generate a ranking $[r_1, r_2, \dots, r_n]$ of shoe models from a reference database of tread depth maps with shoe**

model tags where r_i is more likely to be the shoe model that left a crime-scene shoeprint than r_j for all $i < j$ by learning a representation from a dataset of tread depth maps and clean, fully-visible prints. This requires (1) addressing the domain gap between crime-scene shoeprints and clean prints, and (2) matching patterns to corresponding locations of shoe treads.

3.2 Evaluation Protocol

To benchmark methods, we introduce two validation sets of crime-scene shoeprints with ground-truth shoe model labels, which are linked to a large-scale reference database (see details in Sec. 4.2). Note that the ground-truth for a shoeprint may contain multiple shoe models since tread patterns can be shared by different shoe models. In practice, we expect crime-scene investigators to look through the top K retrieved shoe models and we set K to be a realistically small value of 100, representing the top 0.4% shoe models in our reference database. We use two metrics to compare models based on their top K retrievals. Our first metric, mean average precision at K (mAP@ K), is a standard metric to compare ranking performance. It considers both the number of positive matches and their positions in the ranking list. The second metric, hit ratio at K (hit@ K), is more intuitive and represents the fraction of times we get at least one positive match in the top K retrievals. This metric is useful because a positive match can be used in a query expansion step to retrieve other good matches much more effectively [20]. Both metrics have values between 0 and 1, with higher numbers representing better performance. The supplement has further details.

4 Dataset Preparation

We train our model on a dataset (train-set) of aligned shoe tread depth maps and clean shoeprints. To study the effectiveness of models, we introduce a large-scale reference database (ref-db) of tread depth maps, along with two validation sets (val-FID and val-ShoeCase) created by reprocessing existing datasets of crime-scene shoeprints [29, 47]. We match shoeprints from the validation sets to ref-db and add labels connecting shoeprints in val-FID and val-ShoeCase to ref-db to enable quantitative analysis. An overview of the datasets is provided in Fig. 2, while Fig. 3 and Fig. 4 present example depth maps, clean prints, and crime-scene prints. In this section, we elaborate on our training dataset (train-set), reference database (ref-db), and validation sets (val-FID and val-ShoeCase).

4.1 Online Shoe Tread Depth Maps and Prints for Training

Train-set. Online retailers [1, 2] showcase images of shoe treads for advertisement. Our training set (train-set) contains depth maps and clean, fully visible prints from such tread images as predicted by [43]. We also apply segmentation masks as determined by [43] to the predictions. To ensure consistency across all images, we employ a global alignment method to minimize variations in scale,

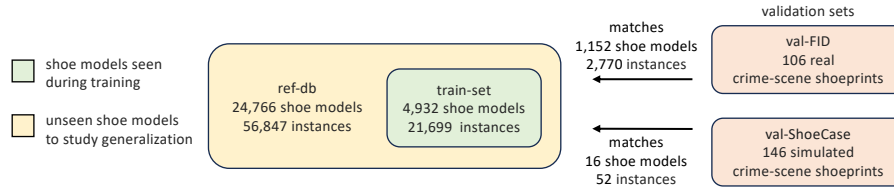


Fig. 2: Dataset statistics. We have a reference database (ref-db) and two validation sets (val-FID and val-ShoeCase) with crime-scene impressions to query against ref-db. We use a section of ref-db for training (train-set) and leave the rest to study generalization. Ground-truth labels from our validation sets connect our query crime-scene shoeprints to shoes in ref-db. See details in Sec. 4 and visual examples in Fig. 3 and 4.

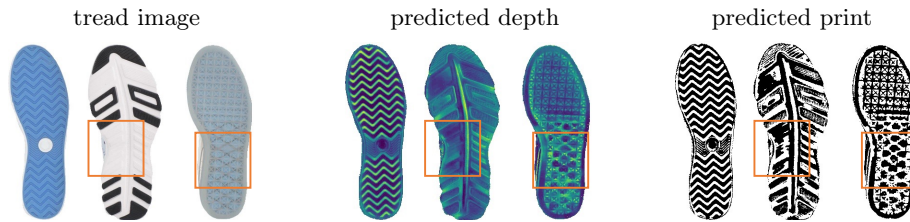


Fig. 3: Examples from train-set. We create training data by leveraging shoe-tread images available from online retailers and predicting their depth maps and prints as outlined in [43]. Note that the depth and print predictions are not always accurate (2nd and 3rd shoe).

orientation, and center using a simple model. Sample shoe-tread images along with their corresponding depth and print predictions are illustrated in Fig. 3. Online retailers categorize shoe styles using stock keeping units (SKUs), which we use as shoe model labels. Shoes with the same SKUs can have different colors and sizes. Sometimes different shoe models can share the same tread pattern.

Statistics. Train-set contains 21,699 shoe instances from 4,932 different shoe models. Each shoe model in our database can have shoe-tread images from multiple shoe instances, possibly with variations in size, color, and lighting. The tread images in train-set have a resolution of 384x192.

Inaccuracies. It is important to note that the training dataset can have some inaccuracies since it comes from raw data downloaded from online retailers. Some tread images might have incorrect model labels, and some images may not depict shoe treads. Other inaccuracies come from imperfect depth and print prediction (cf. Fig. 3), segmentation errors, and alignment failures. We hope to mitigate the errors by including multiple instances per shoe model in train-set.

4.2 Reference Database and Crime-scene Shoeprints for Validation

Ref-db. We introduce a reference database (ref-db) by extending train-set to include more shoe models. The added shoe models are used to study generalization to unseen shoe models. Ref-db contains a total of 56,847 shoe instances

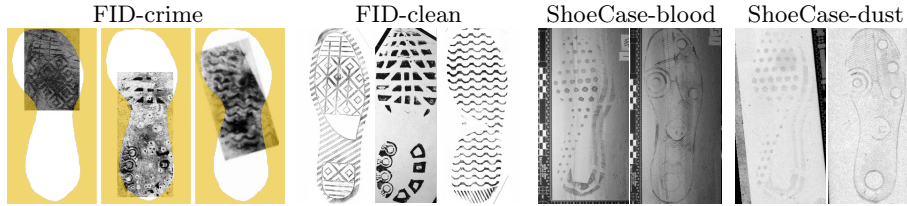


Fig. 4: Examples from val-FID and val-ShoeCase. Val-FID contains real crime-scene shoeprints (FID-crime) and clean, fully visible lab impressions (FID-clean). We show FID-crime and FID-clean shoeprints corresponding to the same shoe models for easier comparison. Note that we show a yellow shoe outline on the FID-crime prints for visualization purposes and the outline does not exist in FID-crime images. Val-ShoeCase contains simulated crime-scene shoeprints on blood (ShoeCase-blood) and dust (ShoeCase-dust). All val-ShoeCase prints are full-sized, as opposed to val-FID.

from 24,766 different shoe models. The inclusion of multiple instances per shoe model in ref-db allows the depth predictor some margin for error (cf. Fig. 3), ensuring minimal impact on the overall matching algorithm performance since it has multiple chances to match a query print to a shoe model. The supplement has details on the distribution of shoe models from our validation sets in ref-db.

Val-FID. We reprocess the widely used FID300 [29] to create our primary validation set (val-FID). Val-FID contains real crime-scene shoeprints (FID-crime) and a corresponding set of clean, fully visible lab impressions (FID-clean). Examples of these prints are shown in Fig. 4. The FID-crime prints are noisy and often only partially visible. It contains impressions made by blood, dust, etc on various kinds of surfaces including hard floors and soft sand. To ensure alignment with ref-db, we preprocess FID-crime prints by placing the partial prints in the appropriate position on a shoe “outline” (cf. Fig. 4), a common practice in shoeprint matching during crime investigations.

We manually found matches to 41 FID-clean prints in ref-db by visual inspection. These are all unique tread patterns and correspond to 106 FID-crime prints. Given that multiple shoe models in ref-db can share the same tread pattern, we store a list of target labels for each shoeprint in FID-crime. These labels correspond to 1,152 shoe models and 2,770 shoe instances in ref-db (cf. Fig. 2).

Val-ShoeCase. We introduce a second validation set (val-ShoeCase) by reprocessing ShoeCase [47] which consists of simulated crime-scene shoeprints made by blood (ShoeCase-blood) or dust (ShoeCase-dust) as shown in Fig. 4. These impressions are created by stepping on blood spatter or graphite powder and then walking on the floor. The prints in this dataset are full-sized, and we manually align them to match ref-db.

ShoeCase uses two shoe models (Adidas Seeley and Nike Zoom Winflow 4), both of which are included in ref-db. The ground-truth labels we prepare for val-ShoeCase include all shoe models in ref-db with visually similar tread patterns as these two shoe models since we do not penalize models for retrieving shoes with matching tread patterns but different shoe models. Val-ShoeCase labels correspond to 16 shoe models and 52 shoe instances in ref-db (cf. Fig. 2).

5 Methodology

In this section, we introduce *CriSp*, our representation learning framework to match crime-scene shoeprint images S to tread depth maps d . An overview of our training pipeline is shown in Fig. 1. *CriSp* is trained using a dataset of globally aligned tread depth maps d and clean, fully-visible shoeprints s (see details in Sec. 4.1). The main components of our pipeline are a data augmentation module *Aug* to simulate crime-scene shoeprints, an encoder network *Enc* to map depths and prints to a spatial feature representation, and a spatial masking module M to mask out irrelevant portions from partially visible shoeprints.

Data augmentation. Our data augmentation module *Aug* simulates noisy and occluded crime-scene shoeprints (cf. Fig. 4) from clean, fully-visible prints (cf. Fig. 3), denoted as $\hat{S} = Aug(s)$. *Aug* uses 3 kinds of degradations (occlusion, erasure, and noise) as visualized in Fig. 5. Occlusion can be in the form of overlapping prints or random shapes. Erasures achieve the grainy texture of crime-scene prints and noise adds background clutter to the images. Further details are provided in the supplement.

Encoder for spatial features. Our encoder *Enc* maps tread depths d and simulated crime-scene shoeprints \hat{S} to a feature representation z , denoted as $z = Enc(x)$ where $x \in [d, \hat{S}]$. *Enc* consists of a modified ResNet50 [24] with the final pooling and flattening operation removed followed by a couple of convolution layers. *Enc* produces features of shape $[C, H, W]$ where C is the feature length, and H and W are the encoded height and width, respectively. For *CriSp* we set $C = 128$. Since our training data and query prints are globally aligned (cf. Sec. 4), *Enc* allows access to features at each (course) spatial location of the image, facilitating comparisons in corresponding locations of shoe treads. *Enc* has two input channels for depth and print, respectively. It processes only one input at a time and pads the other input channel with zeros.

Spatial feature masking. During training, we simulate partially visible crime-scene shoeprints by applying a random rectangular mask m to query prints. Our feature masking module M applies a corresponding mask to spatial features z to obtain $\bar{z} = M(z, m)$. M resizes mask m to a dimension of $[H, W]$, uses it to zero out spatial features outside the mask, and normalizes the masked features. This allows our model to focus on the visible portion of the prints. While it would make sense to apply mask m to tread depth images as well, we opt not to do this as it would necessitate recomputing all the database depth features for each query print image at inference time, which is not scalable.

Training loss and similarity metric. We train our model using supervised contrastive learning [25], which extends self-supervised contrastive learning to a fully supervised setting to learn from data using labels. For a set of N depth/print pairs $\{d_k, s_k\}_{k=1\dots N}$ from shoe models $\{l_k\}_{k=1\dots N}$ within a batch, and a randomly generated mask m per batch, we compute masked spatial features $\{\bar{z}_i\}_{i=1\dots 2N}$ and corresponding shoe labels $\{\bar{l}_i\}_{i=1\dots 2N}$ where $\bar{z}_{2k} = M(Enc(d_k), m)$, $\bar{z}_{2k+1} = M(Enc(Aug(s_k)), m)$, and $\bar{l}_{2k} = \bar{l}_{2k+1} = l_k$. We treat

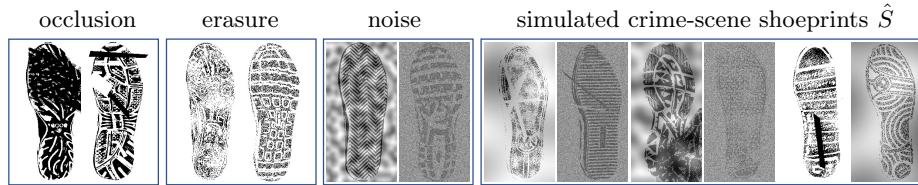


Fig. 5: Examples of data augmentation. Our data augmentation module *Aug* simulates crime-scene shoeprints (cf. Fig. 4) from clean, fully visible prints in our training set (cf. Fig. 3). *Aug* optionally (1) introduces occlusion such as overlapping prints and random shapes, (2) erases parts of the print to create a grainy appearance, and (3) adds noise to mimic background clutter.

\bar{z} as a vector of size CHW and apply the following loss.

$$\mathcal{L} = \sum_{i \in I} \frac{-1}{|P(i)|} \sum_{p \in P(i)} \log \frac{\exp(\bar{z}_i \cdot \bar{z}_p / \tau)}{\sum_{a \in A(i)} \exp(\bar{z}_i \cdot \bar{z}_a / \tau)} \quad (1)$$

Here, $i \in I \equiv \{1 \dots 2N\}$, $A(i) \equiv I \setminus \{i\}$, and $P(i) \equiv \{p \in A(i) : \bar{l}_p = \bar{l}_i\}$ is the set of indices of all positives in the batch distinct from i . $|P(i)|$ is the cardinality of $P(i)$. The \cdot symbol denotes the inner product, and $\tau \in \mathcal{R}^+$ is a scalar temperature parameter. This loss corresponds to using cosine similarity to measure similarity between images.

Sampling. For the above loss to be effective, we must have positive examples for all shoe models within a batch. However, if we pick shoe models randomly from a dataset with a very large number of shoe models, we can expect to sample a set of unique shoe models each time. Then, this loss would act like its self-supervised counterpart. To remedy this, we sample data in pairs, i.e. we choose $N/2$ shoe models randomly and select two shoe instances from each shoe model.

6 Experiments

We evaluate our *CriSp* and compare it with state-of-the-art methods on automated shoeprint matching [26] and image retrieval [25, 31, 42, 51]. We begin with visual comparison and quantitative evaluation, followed by an ablation study and analysis of our design choices. We will open-source our code and dataset to foster research after acceptance of this work.

6.1 Qualitative Results of CriSp

Figure 6 shows the top 10 retrievals of our method *CriSp* on the val-FID and val-ShoeCase datasets. Notable, *CriSp* can retrieve a positive match very early even when the shoeprint has significantly limited visibility or is severely degraded. These retrievals show how *CriSp* effectively matches distinctive patterns from corresponding regions of the tread. Additionally, Fig. 7 shows a comparison with related methods fine-tuned on our dataset. Clearly, *CriSp* performs significantly better at retrieving positive matches early. The supplement has further visualizations.

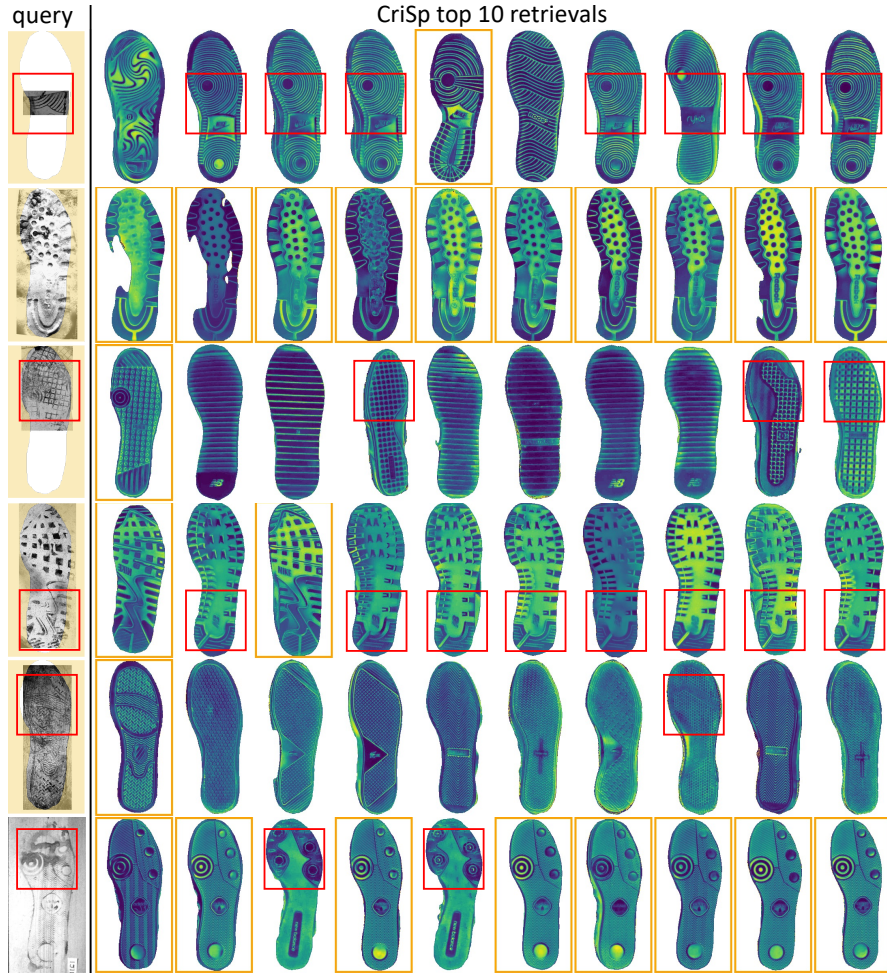


Fig. 6: Visualization of the top 10 retrievals by *CriSp* on val-FID (rows 1-5) and val-ShoeCase (row 6). *CriSp* retrieves positive matches (highlighted in orange) very early even when crime-scene shoeprints have very limited visibility or severe degradation. Additionally, corresponding locations on the retrieved shoes share similar patterns to the query print, even in negative matches (highlighted in red).

6.2 Comparison with State-of-the-art

CriSp consistently outperforms previous methods across most validation examples (details in the supplement). Table 1 and 2 list comparisons on our two evaluation metrics introduced in Sec. 3.2. We analyze these results below.

Comparison with shoeprint matching. MCNCC [26] employs features from pretrained networks on ImageNet for automated shoeprint matching. However, leveraging learning on shoeprint-specific data, *CriSp* exhibits superior performance on both val-FID (see Tab. 1) and val-ShoeCase (see Tab. 2). Although MCNCC proposes to use clean shoeprint impressions as the reference database

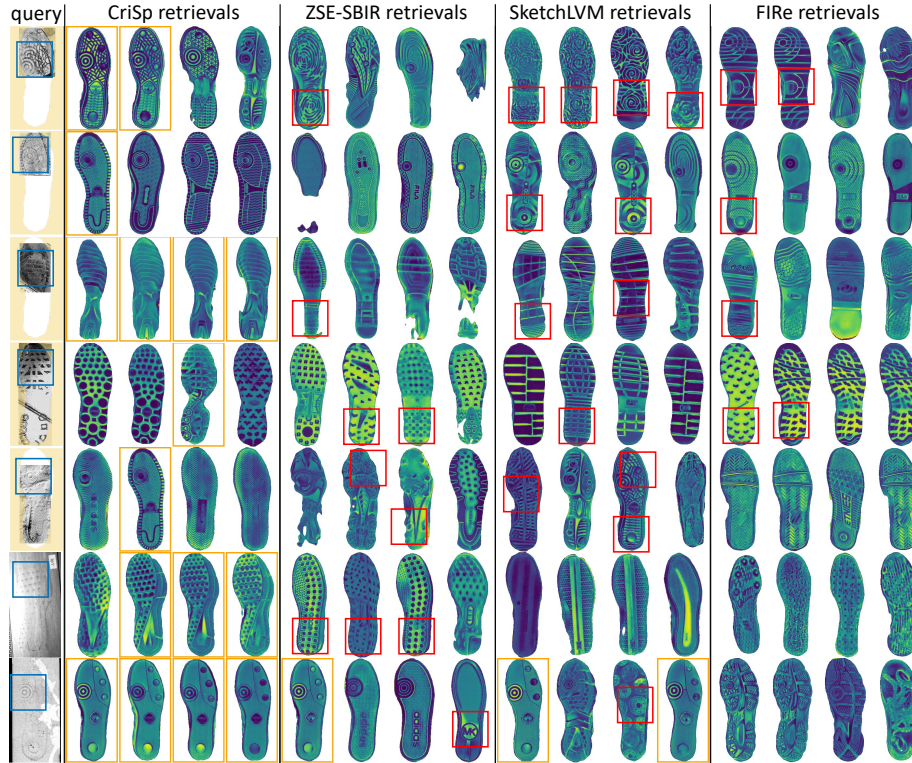


Fig. 7: Qualitative comparison with state-of-the-art methods on val-FID (rows 1-5), val-ShoeCase (rows 6-7). We show the top 4 retrieved results. *CriSp* demonstrates the ability to localize patterns, allowing it to retrieve positive matches (highlighted in orange) much earlier than previous methods. While prior methods identify similar patterns to the query print (highlighted in blue), they cannot determine if they are from corresponding locations, as indicated by the red boxes.

to match with, we use tread depth maps to be consistent with other methods and to achieve enhanced results. The supplement has details.

Comparison with image retrieval. Table 1 and 2 demonstrate how our *CriSp* consistently outperforms state-of-the-art methods in image retrieval (SupCon [25], FIRe [51], SketchLVM [42], ZSE-SBIR [31]). We fine-tune these methods on our training data containing tread depth maps and clean, fully-visible shoeprints. Additionally, we use our data augmentation module *Aug* to simulate crime-scene shoeprints while training prior methods as the wide domain gap between crime-scene prints and the training data causes them to perform poorly otherwise (cf. Tab. 1). Even when prior methods use our data augmentation, *CriSp* significantly outperforms them on both val-FID (Tab. 1) and val-ShoeCase (Tab. 2). The ablation study (Tab. 5) shows that our spatial feature masking technique greatly improves the performance. Qualitative comparison on both validation sets in Fig. 7 also confirm that *CriSp* is better able to match shoeprint patterns to corresponding locations on tread depth maps, thus making

Table 1: Benchmarking on real crime-scene prints from val-FID. We use hit@100 and mAP@100 as our metrics and compare performance with prior methods trained on our dataset both with and without our data augmentation (see details in Sec. 5), which simulates crime-scene shoeprints from clean, fully-visible prints provided in the training data. Since MCNCC [26] uses features from a pretrained network, it cannot be fine-tuned on our data. Clearly, all other prior methods benefit greatly from using our data augmentation technique. Moreover, *CriSp* significantly outperforms all prior methods on both metrics, even when they are trained with our data augmentation.

method	w/o our data aug		w/ our data aug	
	hit@100	mAP@100	hit@100	mAP@100
IJCV'19 MCNCC [26]	0.0849	0.0018	-	-
NeurIPS'20 SupCon [25]	0.0472	0.0020	0.0755	0.0096
ICLR'21 FRe [51]	0.1132	0.0014	0.2075	0.0398
CVPR'23 SketchLVM [42]	0.0849	0.0066	0.1981	0.0384
CVPR'23 ZSE-SBIR [31]	0.0943	0.0065	0.4528	0.1412
CriSp	0.0754	0.0174	0.5472	0.2071

Table 2: Benchmarking on simulated crime-scene prints from val-ShoeCase, which includes prints made by blood and dust. We use hit@100 and ma@100 as our metrics and *CriSp* performs the best across both metrics and print categories. Notably, all prior methods have been fine-tuned on our dataset using our data augmentation technique, as they perform poorly otherwise (cf. Tab. 1).

method	ShoeCase-blood		ShoeCase-dust	
	hit@100	mAP@100	hit@100	mAP@100
MCNCC [26]	0.0000	0.0000	0.0000	0.0000
SupCon [25]	0.0000	0.0000	0.0000	0.0000
FRe [51]	0.3896	0.0275	0.8194	0.3779
SketchLVM [42]	0.6623	0.1058	0.5972	0.2696
ZSE-SBIR [31]	0.8052	0.1849	0.9444	0.4063
CriSp	0.8052	0.4355	0.9444	0.6792

positive retrievals early. This is reflected by our mAP@100 values when compared to prior methods on both validation sets (Tab. 1 and 2).

Scalability. In practice, when dealing with a large reference database, scalability becomes crucial. Unlike our closest competitor ZSE-SBIR [31], which necessitates the recomputation of all database features for each query, *CriSp* offers a scalable solution. It can precompute spatial database features and efficiently perform feature masking and cosine similarity calculations for each query, enabling rapid retrieval even with extensive reference databases.

Simulating partial print. Retrievals by prior methods on partial shoeprints in Fig. 7 reveal instances of poorly segmented tread depth maps, where significant portions of the tread pattern have been erased. This raises the question of whether prior methods would exhibit improved performance if trained with masks simulating partial prints. However, it's worth noting that prior methods perform better when trained without such masks, as detailed in the supplement.

Table 3: Testing database image configurations. The hit@100 and mAP@100 values for FID-clean shoeprints indicate that using only tread depth as the database image configuration yields the best performance. Results for FID-crime are not reported in this experiment as we do not simulate crime-scene prints.

Database config.		FID-clean	
RGB depth	print	hit@100	mAP@100
✓		0.195	0.066
	✓	0.512	0.203
		0.171	0.015
✓	✓	0.293	0.057

Table 4: Effect of our data augmentation. We train a ResNet50 with our data augmentation and report hit@100 and mAP@100 values for FID-crime shoeprints. Our results confirm that each component of our data augmentation (visualized in Fig. 5) individually improves retrieval results and performs best when used together.

Data augmentation			FID-crime	
occlusion	erasure	noise	hit@100	mAP@100
			0.009	0.0000
✓			0.019	0.0003
	✓		0.075	0.0098
		✓	0.170	0.0241
✓	✓	✓	0.226	0.0520

Val-FID vs val-ShoeCase. Methods show a wider variation in performance on Val-ShoeCase than val-FID. This discrepancy arises from the fact that val-FID contains the diversity of real crime-scene shoeprints, while val-ShoeCase systematically simulates crime-scene prints. Additionally, val-ShoeCase contains prints from shoe models with only two unique tread patterns while val-FID contains prints from 41 unique tread patterns (cf. Sec. 4.2).

6.3 Design Choices and Ablation Study

We conduct a study of our design choices by training a ResNet50 with a supervised contrastive loss and then sequentially adding modules to investigate their performance impact. Specifically, we analyze database image configurations, data augmentation techniques, and spatial feature masking.

Database image configuration. We start by testing the effectiveness of different types of database image configurations (RGB tread images, depth, and print). Our analysis shows that depth is the most relevant and informative modality, yielding the best results when used alone (Tab. 3). Print can be derived from depth by thresholding [43] and the extra information in rgb tread images (lighting and albedo) can be distracting.

Data augmentation. Next, we test the effectiveness of each component of our data augmentation technique. Table 4 shows that all 3 components contribute to improved performance and work best when used together, bringing our hit@100 and mAP@100 on FID-crime to (0.226, 0.0520) from (0.009, 0.000).

Spatial features and feature masking. With our data augmentation in place, we study the effect of spatial feature masking, which helps *CriSp* match query print patterns to the relevant spatial locations of the database tread depth maps. Table 5 shows the influence of using spatial features and feature masking. Our findings indicate that spatial features, feature masking, and query image masking during training all contribute greatly to improving performance.

Table 5: Effect of spatial features and feature masking. We validate the effect of using spatial features and applying feature masking on both our encoder *Enc*, which incorporates spatial features during training, and on a pretrained ResNet50 trained with our data augmentation (cf. Tab. 4). For ResNet50, which does not utilize spatial features during training, we obtain spatial features by removing the last pooling operation. We present results for FID-crime shoeprints from val-FID using hit@100 and mAP@100 metrics. Using spatial features from a pretrained ResNet50 boosts retrieval performance. Additionally, masking the spatial features improves performance further for both the ResNet50 and our *Enc*. Furthermore, adding query print masking during training further boosts performance to hit@100=0.5472 and mAP@100=0.2071.

encoder	train w/ spatial feat.	spatial features	mask features	mask query print	FID-crime	
					hit@100	mAP@100
ResNet50					0.2264	0.0520
ResNet50		✓			0.3585	0.0863
ResNet50		✓	✓		0.4245	0.1212
<i>Enc</i>	✓	✓			0.3774	0.1137
<i>Enc</i>	✓	✓	✓		0.4528	0.1765
<i>Enc</i>	✓	✓	✓	✓	0.5472	0.2071

7 Discussions and Conclusions

Limitations. While *CriSp* significantly outperforms prior methods on this problem, it still has some limitations. We use CNNs since it is straightforward to localize pattern matching to corresponding locations on images by applying spatial feature masking. However, pairing localization techniques with more sophisticated models such as vision transformers is expected to perform better. We also assume that the crime-scene shoeprints are manually aligned before queries are made. Methods that do not require this step are easier to use.

Potential negative impact. We introduce a method to aid in forensic investigations. However, if investigators tend to rely *solely* on our retrievals for crime-scene shoeprint identification, then criminals wearing shoe models that are not well-represented by *CriSp* would become harder to identify. We have to always consider the possibility that the shoe model that left a crime-scene impression may not be present in the top retrievals.

Conclusion. In this paper, we propose a method to retrieve and rank the closest matches to crime-scene shoeprints from a database of shoe tread images. This is a socially important problem and helps forensic investigations. We introduce a way to learn from large-scale data and propose a spatial feature masking method to localize the search for patterns over the shoe tread. Our method consistently outperforms the state-of-the-art on both image retrieval and crime-scene shoeprint matching methods on our two validation sets that we reprocess from the widely used FID and more recent ShoeCase datasets. Future explorations can investigate using architectures like vision transformers and extend the problem to when alignment is not guaranteed.

Acknowledgements. This work was funded by the Center for Statistics and Applications in Forensic Evidence (CSAFE) through Cooperative Agreements, 70NANB15H176 and 70NANB20H019.

References

1. 6pm, <http://www.6pm.com> 5
2. Zappos, <http://www.zappos.com> 5
3. AlGarni, G., Hamiane, M.: A novel technique for automatic shoeprint image retrieval. *Forensic science international* **181**(1-3), 10–14 (2008) 2, 3
4. Alizadeh, S., Kose, C.: Automatic retrieval of shoeprint images using blocked sparse representation. *Forensic science international* **277**, 103–114 (2017) 2, 3
5. Almaadeed, S., Bouridane, A., Crookes, D., Nibouche, O.: Partial shoeprint retrieval using multiple point-of-interest detectors and sift descriptors. *Integrated Computer-Aided Engineering* **22**(1), 41–58 (2015) 2, 3
6. Arandjelovic, R., Gronat, P., Torii, A., Pajdla, T., Sivic, J.: Netvlad: Cnn architecture for weakly supervised place recognition. In: *Proceedings of the IEEE conference on computer vision and pattern recognition*. pp. 5297–5307 (2016) 4
7. Babenko, A., Lempitsky, V.: Aggregating deep convolutional features for image retrieval. *arXiv preprint arXiv:1510.07493* (2015) 4
8. Babenko, A., Slesarev, A., Chigorin, A., Lempitsky, V.: Neural codes for image retrieval. In: *Computer Vision–ECCV 2014: 13th European Conference, Zurich, Switzerland, September 6-12, 2014, Proceedings, Part I 13*. pp. 584–599. Springer (2014) 4
9. Bay, H., Ess, A., Tuytelaars, T., Van Gool, L.: Speeded-up robust features (surf). *Computer vision and image understanding* **110**(3), 346–359 (2008) 3
10. Beis, J.S., Lowe, D.G.: Shape indexing using approximate nearest-neighbour search in high-dimensional spaces. In: *Proceedings of IEEE computer society conference on computer vision and pattern recognition*. pp. 1000–1006. IEEE (1997) 4
11. Bodziak, W.J.: *Footwear impression evidence: detection, recovery, and examination*. CRC Press (2017) 1
12. Bouridane, A., Alexander, A., Nibouche, M., Crookes, D.: Application of fractals to the detection and classification of shoeprints. In: *Proceedings 2000 International Conference on Image Processing (Cat. No. 00CH37101)*. vol. 1, pp. 474–477. IEEE (2000) 2
13. Cao, B., Araujo, A., Sim, J.: Unifying deep local and global features for image search. In: *Computer Vision–ECCV 2020: 16th European Conference, Glasgow, UK, August 23–28, 2020, Proceedings, Part XX 16*. pp. 726–743. Springer (2020) 4
14. Chowdhury, P.N., Bhunia, A.K., Sain, A., Koley, S., Xiang, T., Song, Y.Z.: Scenetrilogy: On human scene-sketch and its complementarity with photo and text. In: *Proceedings of the IEEE/CVF Conference on Computer Vision and Pattern Recognition*. pp. 10972–10983 (2023) 4
15. Datta, A.K., Lee, H.C., Ramotowski, R., Gaensslen, R.: *Advances in fingerprint technology*. CRC press (2001) 3
16. De Chazal, P., Flynn, J., Reilly, R.B.: Automated processing of shoeprint images based on the fourier transform for use in forensic science. *IEEE transactions on pattern analysis and machine intelligence* **27**(3), 341–350 (2005) 2

17. Deng, J., Dong, W., Socher, R., Li, L.J., Li, K., Fei-Fei, L.: Imagenet: A large-scale hierarchical image database. In: 2009 IEEE conference on computer vision and pattern recognition. pp. 248–255. Ieee (2009) [2](#), [3](#)
18. Dey, S., Riba, P., Dutta, A., Lladós, J., Song, Y.Z.: Doodle to search: Practical zero-shot sketch-based image retrieval. In: Proceedings of the IEEE/CVF conference on computer vision and pattern recognition. pp. 2179–2188 (2019) [4](#)
19. Dutta, A., Akata, Z.: Semantically tied paired cycle consistency for zero-shot sketch-based image retrieval. In: Proceedings of the IEEE/CVF Conference on Computer Vision and Pattern Recognition. pp. 5089–5098 (2019) [4](#)
20. Efthimiadis, E.N.: Query expansion. Annual review of information science and technology (ARIST) **31**, 121–87 (1996) [5](#)
21. Gordo, A., Almazán, J., Revaud, J., Larlus, D.: Deep image retrieval: Learning global representations for image search. In: Computer Vision–ECCV 2016: 14th European Conference, Amsterdam, The Netherlands, October 11–14, 2016, Proceedings, Part VI 14. pp. 241–257. Springer (2016) [4](#)
22. Gueham, M., Bouridane, A., Crookes, D.: Automatic recognition of partial shoeprints based on phase-only correlation. In: 2007 IEEE International Conference on Image Processing. vol. 4, pp. IV–441. IEEE (2007) [2](#)
23. Han, X., Leung, T., Jia, Y., Sukthankar, R., Berg, A.C.: Matchnet: Unifying feature and metric learning for patch-based matching. In: Proceedings of the IEEE conference on computer vision and pattern recognition. pp. 3279–3286 (2015) [4](#)
24. He, K., Zhang, X., Ren, S., Sun, J.: Deep residual learning for image recognition. In: Proceedings of the IEEE conference on computer vision and pattern recognition. pp. 770–778 (2016) [8](#)
25. Khosla, P., Teterwak, P., Wang, C., Sarna, A., Tian, Y., Isola, P., Maschinot, A., Liu, C., Krishnan, D.: Supervised contrastive learning. Advances in neural information processing systems **33**, 18661–18673 (2020) [4](#), [8](#), [9](#), [11](#), [12](#), [21](#), [26](#)
26. Kong, B., Supancic III, J., Ramanan, D., Fowlkes, C.C.: Cross-domain image matching with deep feature maps. International Journal of Computer Vision **127**(11), 1738–1750 (2019) [2](#), [3](#), [9](#), [10](#), [12](#), [19](#), [21](#), [26](#)
27. Kong, X., Yang, C., Zheng, F.: A novel method for shoeprint recognition in crime scenes. In: Biometric Recognition: 9th Chinese Conference, CCBR 2014, Shenyang, China, November 7–9, 2014. Proceedings 9. pp. 498–505. Springer (2014) [2](#), [3](#)
28. Kortylewski, A., Albrecht, T., Vetter, T.: Unsupervised footwear impression analysis and retrieval from crime scene data. In: Computer Vision-ACCV 2014 Workshops: Singapore, Singapore, November 1–2, 2014, Revised Selected Papers, Part I 12. pp. 644–658. Springer (2015) [2](#), [3](#)
29. Kortylewski, A., Albrecht, T., Vetter, T.: Unsupervised footwear impression analysis and retrieval from crime scene data. In: Computer Vision-ACCV 2014 Workshops: Singapore, Singapore, November 1–2, 2014, Revised Selected Papers, Part I 12. pp. 644–658. Springer (2015) [2](#), [5](#), [7](#)
30. Krizhevsky, A., Sutskever, I., Hinton, G.E.: Imagenet classification with deep convolutional neural networks. Advances in neural information processing systems **25** (2012) [4](#)
31. Lin, F., Li, M., Li, D., Hospedales, T., Song, Y.Z., Qi, Y.: Zero-shot everything sketch-based image retrieval, and in explainable style. In: Proceedings of the IEEE/CVF Conference on Computer Vision and Pattern Recognition. pp. 23349–23358 (2023) [4](#), [9](#), [11](#), [12](#), [21](#), [26](#)
32. Lowe, D.G.: Distinctive image features from scale-invariant keypoints. International journal of computer vision **60**, 91–110 (2004) [3](#)

33. Ma, Z., Ding, Y., Wen, S., Xie, J., Jin, Y., Si, Z., Wang, H.: Shoe-print image retrieval with multi-part weighted cnn. *IEEE Access* **7**, 59728–59736 (2019) [2](#), [3](#)
34. Nister, D., Stewenius, H.: Scalable recognition with a vocabulary tree. In: 2006 IEEE Computer Society Conference on Computer Vision and Pattern Recognition (CVPR'06). vol. 2, pp. 2161–2168. Ieee (2006) [4](#)
35. Noh, H., Araujo, A., Sim, J., Weyand, T., Han, B.: Large-scale image retrieval with attentive deep local features. In: Proceedings of the IEEE international conference on computer vision. pp. 3456–3465 (2017) [4](#)
36. Pang, K., Song, Y.Z., Xiang, T., Hospedales, T.M.: Cross-domain generative learning for fine-grained sketch-based image retrieval. In: BMVC. pp. 1–12 (2017) [4](#)
37. Philbin, J., Chum, O., Isard, M., Sivic, J., Zisserman, A.: Object retrieval with large vocabularies and fast spatial matching. In: 2007 IEEE conference on computer vision and pattern recognition. pp. 1–8. IEEE (2007) [4](#)
38. Qian, Y., Feng, L., Song, Y., Tao, X., Chen, C.L.: Sketch me that shoe. In: IEEE Conf. Comput. Vision and Pattern Recognit.(CVPR). pp. 799–807 (2016) [4](#)
39. Radenović, F., Tolias, G., Chum, O.: Cnn image retrieval learns from bow: Unsupervised fine-tuning with hard examples. In: Computer Vision–ECCV 2016: 14th European Conference, Amsterdam, The Netherlands, October 11–14, 2016, Proceedings, Part I 14. pp. 3–20. Springer (2016) [4](#)
40. Radenović, F., Tolias, G., Chum, O.: Fine-tuning cnn image retrieval with no human annotation. *IEEE transactions on pattern analysis and machine intelligence* **41**(7), 1655–1668 (2018) [4](#)
41. Rida, I., Fei, L., Proenca, H., Nait-Ali, A., Hadid, A.: Forensic shoe-print identification: a brief survey. arXiv preprint arXiv:1901.01431 (2019) [3](#)
42. Sain, A., Bhunia, A.K., Chowdhury, P.N., Koley, S., Xiang, T., Song, Y.Z.: Clip for all things zero-shot sketch-based image retrieval, fine-grained or not. In: Proceedings of the IEEE/CVF Conference on Computer Vision and Pattern Recognition. pp. 2765–2775 (2023) [4](#), [9](#), [11](#), [12](#), [21](#), [26](#)
43. Shafique, S., Kong, B., Kong, S., Fowlkes, C.: Creating a forensic database of shoeprints from online shoe-tread photos. In: Proceedings of the IEEE/CVF Winter Conference on Applications of Computer Vision. pp. 858–868 (2023) [2](#), [3](#), [5](#), [6](#), [13](#), [19](#)
44. Sharif Razavian, A., Azizpour, H., Sullivan, J., Carlsson, S.: Cnn features off-the-shelf: an astounding baseline for recognition. In: Proceedings of the IEEE conference on computer vision and pattern recognition workshops. pp. 806–813 (2014) [4](#)
45. Song, J., Song, Y.Z., Xiang, T., Hospedales, T.M.: Fine-grained image retrieval: the text/sketch input dilemma. In: BMVC. vol. 2, p. 7 (2017) [4](#)
46. Song, J., Yu, Q., Song, Y.Z., Xiang, T., Hospedales, T.M.: Deep spatial-semantic attention for fine-grained sketch-based image retrieval. In: Proceedings of the IEEE international conference on computer vision. pp. 5551–5560 (2017) [4](#)
47. Tibben, A., McGuire, M., Renfro, S., Carriquiry, A.: Shoecase: A data set of mock crime scene footwear impressions. *Data in Brief* **50**, 109546 (2023) [5](#), [7](#)
48. Tolias, G., Avrithis, Y., Jégou, H.: Image search with selective match kernels: aggregation across single and multiple images. *International Journal of Computer Vision* **116**, 247–261 (2016) [4](#)
49. Tolias, G., Sivic, R., Jégou, H.: Particular object retrieval with integral max-pooling of cnn activations. arXiv preprint arXiv:1511.05879 (2015) [4](#)
50. Wei, C.H., Gwo, C.Y.: Alignment of core point for shoeprint analysis and retrieval. In: 2014 International Conference on Information Science, Electronics and Electrical Engineering. vol. 2, pp. 1069–1072. IEEE (2014) [2](#), [3](#)

51. Weinzaepfel, P., Lucas, T., Larlus, D., Kalantidis, Y.: Learning super-features for image retrieval. In: International Conference on Learning Representations (2021) [4](#), [9](#), [11](#), [12](#), [21](#), [26](#)
52. Yelamarthi, S.K., Reddy, S.K., Mishra, A., Mittal, A.: A zero-shot framework for sketch based image retrieval. In: Proceedings of the European Conference on Computer Vision (ECCV). pp. 300–317 (2018) [4](#)
53. Zhang, Y., Fu, H., Dellandréa, E., Chen, L.: Adapting convolutional neural networks on the shoeprint retrieval for forensic use. In: Chinese Conference on Biometric Recognition. pp. 520–527. Springer (2017) [2](#), [3](#)
54. Zheng, L., Yang, Y., Tian, Q.: Sift meets cnn: A decade survey of instance retrieval. IEEE transactions on pattern analysis and machine intelligence **40**(5), 1224–1244 (2017) [3](#)

Appendix

8 Outline

Our aim is to identify shoe models resembling crime-scene impressions by comparing them to a comprehensive shoe database. Leveraging tread images from online retailers, we construct our reference database, prioritizing tread depth maps over RGB tread images for their greater relevance and informativeness [43]. As there is no dataset of crime-scene shoeprints paired with ground-truth tread depth maps, we propose learning from tread depth maps and clean shoeprints predicted from RGB tread images instead. We utilize a data augmentation module *Aug* to bridge the domain gap between clean and crime-scene prints, and a spatial feature masking strategy (using spatial encoder *Enc* and masking module *M*) to match shoeprint patterns with corresponding locations on tread depth maps. *CriSp* achieves significantly better retrieval results than prior methods.

In this supplementary document, we discuss the following topics:

- Section 9 presents visualizations of retrievals by *CriSp* and also compares them with those of prior methods.
- Section 10 provides a detailed quantitative comparison to state-of-the-art methods. We study generalization to unseen shoe models in Sec. 10.1 and further detail the performance of methods on each unique shoe tread pattern in Sec. 10.2.
- Section 11 elaborates on the training process of prior methods. We investigate the performance of fine-tuning these methods using masks to simulate partial prints in Sec. 11.1 and compare the performance of MCNCC [26] when using a reference database of shoeprints vs. tread depth maps in Sec. 11.2.
- Section 12 defines the mean average precision at K, which serves as a metric for evaluating and comparing methods.
- Section 13 analyses how the ground-truth shoe models are distributed within our reference database.
- Section 14 provides detailed insights into our data augmentation technique.
- Section 15 shares some implementation specifics of *CriSp*.

9 Qualitative Results of *CriSp* and Comparison to State-of-the-art

We display visualizations in this section. Figure 8 and 9 show the top 10 retrievals by *CriSp* from crime-scene prints sourced from val-FID and val-ShoeCase, respectively. These illustrations demonstrate *CriSp*'s capability to retrieve positive matches even from severely degraded or partially visible crime-scene shoeprints.

Table 6: Distribution of ground-truth shoe models from validation sets (val-FID and val-ShoeCase). We partition the ground-truth shoe models to assess generalization capabilities. In val-FID, there are 1152 shoe models, while val-ShoeCase comprises 16 shoe models. It’s important to note that different shoe models may share tread patterns. Thus, we also distinguish between seen and unseen tread patterns during training. Val-FID encompasses 41 unique tread patterns, whereas val-ShoeCase contains 2 unique tread patterns.

	shoe models			unique tread patters		
	seen	unseen	total	seen	unseen	total
val-FID	229	923	1152	20	21	41
val-ShoeCase	2	14	16	1	1	2

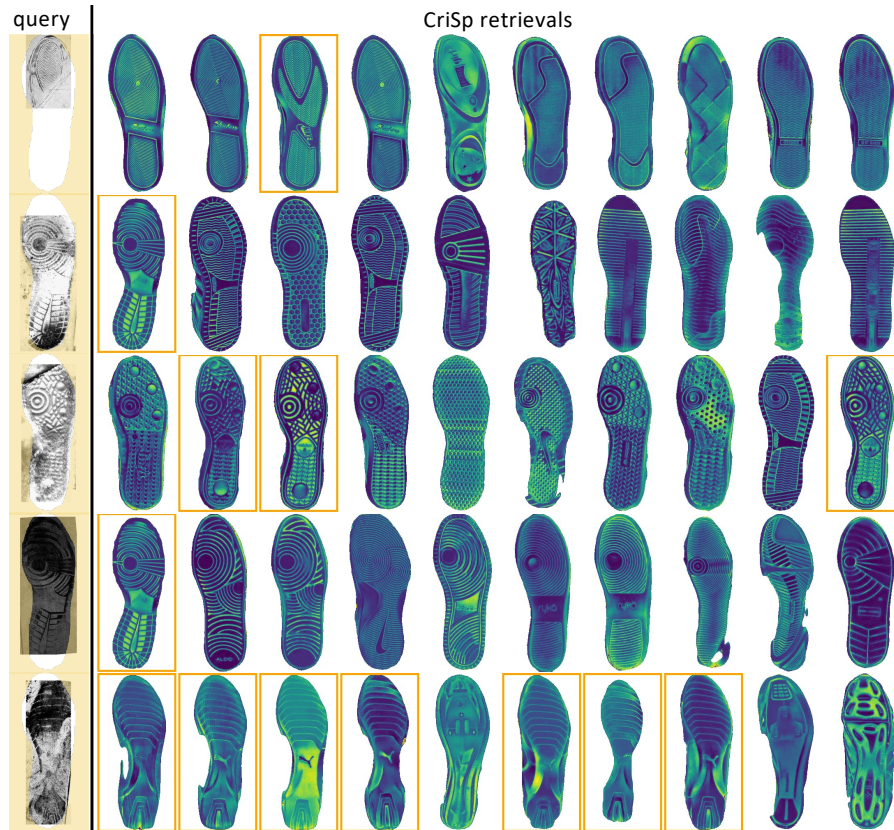


Fig. 8: Qualitative results of *CriSp* on val-FID. *CriSp* retrieves positive matches early even with partially visible or severely degraded prints.

Furthermore, Figure 10 and 11 provide a qualitative comparison between retrievals made by *CriSp* and those of prior methods. Notably, *CriSp* excels in

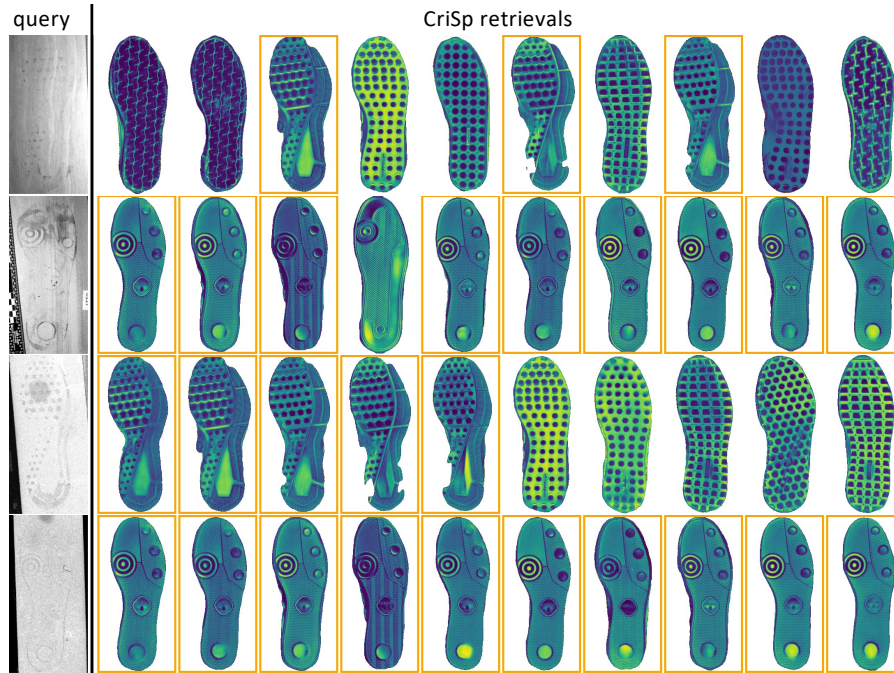


Fig. 9: Qualitative results of *CriSp* on val-ShoeCase. We show the performance on prints from two different categories: blood prints (rows 1-2) and dust prints (rows 3-4). Despite the severe degradation present in the prints, *CriSp* can retrieve positive matches early.

Table 7: Benchmarking on validation sets to study generalization. We train prior methods on our dataset with our data augmentation technique. We compare the retrieval performance of methods using mAP@100. We categorize the shoeprints in the validation sets based on whether their corresponding tread patterns were seen during training or not. Note that we perform this study in terms of seen and unseen tread patterns instead of shoe models since multiple shoe models can share the same tread pattern. Notably, *CriSp* demonstrates significantly superior performance to all prior methods on unseen tread patterns. However, ZSE-SBIR exhibits slightly better performance than *CriSp* for seen tread patterns on val-ShoeCase.

method	val-FID		val-ShoeCase	
	seen	unseen	seen	unseen
IJCV'19 MCNCC [26]	0.0002	0.0030	0.0000	0.0000
NeurIPS'20 SupCon [25]	0.0009	0.0000	0.0000	0.0000
ICLR'21 FIRE [51]	0.0671	0.0198	0.1103	0.2697
CVPR'23 SketchLVM [42]	0.0539	0.0270	0.0032	0.2770
CVPR'23 ZSE-SBIR [31]	0.1659	0.1230	0.2653	0.1350
CriSp	0.1749	0.2309	0.2495	0.4405

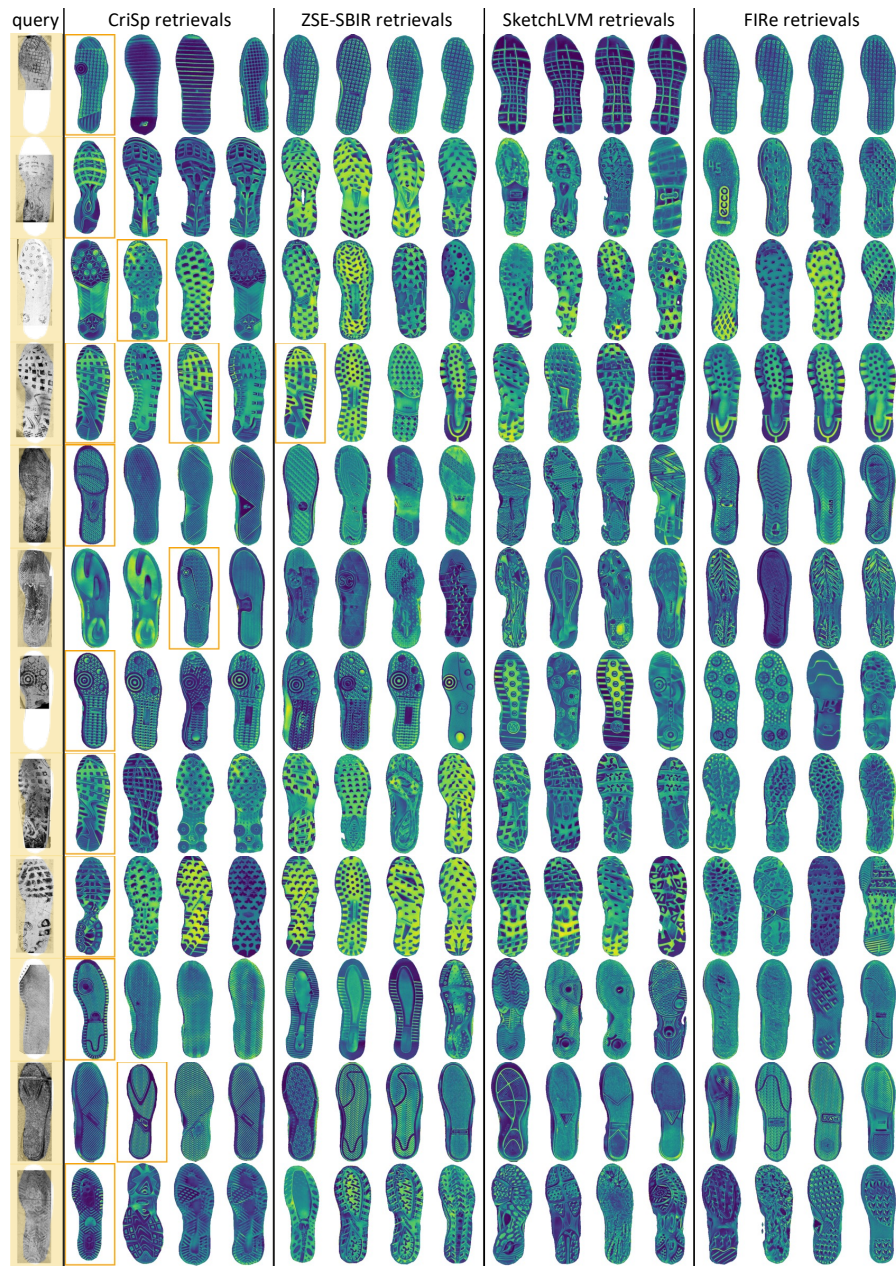


Fig. 10: Qualitative comparison to state-of-the-art on val-FID. *CriSp* outperforms prior methods by retrieving positive matches much earlier.



Fig. 11: Qualitative comparison to state-of-the-art on val-ShoeCase. *CriSp* outperforms prior methods by retrieving positive matches earlier, as evidenced by the top 6 rows displaying blood prints and the bottom 6 rows displaying dust prints.

Table 8: We show mAP@100 for all unique tread patterns in val-FID. *CriSp* achieves the highest performance on 22 tread patterns, while ZSE-SBIR outperforms on 10 tread patterns. FIRE and SketchLVM exhibit the best performance on 1 tread pattern each.

tread pattern ID	FIRE	SketchLVM	ZSE-SBIR	CriSp
000001	0.0000	0.0000	0.2583	0.0027
000003	0.0000	0.0000	0.0079	0.2333
000004	0.3108	0.0000	0.6137	0.6430
000005	0.1694	0.2083	0.5000	0.4105
000008	0.0025	0.0010	0.0034	0.0616
000009	0.0000	0.0000	0.0053	0.0000
000010	0.0000	0.0000	0.0250	0.5000
000011	0.0000	0.0000	0.4275	0.5060
000012	0.0067	0.0022	0.0713	0.0854
000013	0.0348	0.1145	0.2401	0.0111
000016	0.0000	0.0000	0.0563	0.0707
000017	0.1641	0.0227	0.0105	0.0118
000023	0.0000	0.3950	0.0009	0.0148
000032	0.0000	0.0000	0.0000	0.0000
000033	0.0000	0.0000	0.2969	0.5711
000035	0.0000	0.0002	0.0027	0.0000
000045	0.0147	0.0000	0.0000	0.2500
000047	0.0000	0.0066	0.0000	0.0312
000053	0.0156	0.0000	0.0029	0.0427
000054	0.3148	0.0000	0.9444	0.0265
000055	0.0000	0.0000	0.0000	0.3258
000056	0.0000	0.0000	0.0000	0.0000
000062	0.0000	0.0000	0.0000	0.0000
000072	0.0018	0.0140	0.0054	0.0821
000074	0.0000	0.0000	0.0000	1.0000
000082	0.0000	0.0000	0.0000	0.0026
001040	0.0029	0.0000	0.0460	0.0044
001041	0.0000	0.0034	0.0027	0.2000
001044	0.2640	0.3070	0.4100	0.5091
001047	0.0000	0.0000	0.0000	0.0000
001048	0.0000	0.0000	0.1036	0.0000
001049	0.0000	0.0100	0.0238	0.8333
001050	0.0038	0.1704	0.0437	0.3410
001058	0.0000	0.0000	0.3998	0.0201
001062	0.0000	0.0000	0.0000	0.4111
001064	0.0000	0.0000	0.0000	0.0006
001071	0.0000	0.0000	0.0000	0.0108
001076	0.0000	0.0000	0.0000	0.0000
001079	0.0000	0.0000	0.0000	0.0000
001088	0.0000	0.0000	0.5000	0.0903
001095	0.0000	0.0000	0.0000	0.0000

matching patterns to corresponding regions on the tread, enabling it to retrieve positive matches early.

10 Detailed Quantitative Comparison to State-of-the-art

10.1 Generalization to Unseen Shoe Models

We compare our *CriSp* to state-of-the-art methods to study generalization to unseen tread patterns. Note that we perform this study in terms of seen and unseen tread patterns instead of shoe models since multiple shoe models can share the same tread pattern. Our findings, detailed in Tab. 7, demonstrate that *CriSp* exhibits superior generalization to unseen tread patterns compared to prior methods.

10.2 Comparison on Unique Tread Patterns

We conduct a detailed analysis of *CriSp* relative to prior methods on each unique tread pattern from val-FID. Recall that val-FID has 41 unique tread patterns among the 1152 ground-truth shoe models. Table 8 presents the comparison of methods based on mAP@100 for each tread pattern, where *CriSp* exhibits superior performance in the majority of cases.

11 Training State-of-the-art Methods

11.1 Fine-tuning State-of-the-art Methods Using Simulated Crime-Scene Masks

When evaluating state-of-the-art methods, we train them on our dataset and apply our data augmentation to simulate crime-scene prints during training. Here, we compare the performance of related methods with and without using masks to simulate partial prints. Our findings are summarized in Tab. 9, demonstrating that *CriSp* outperforms other methods in both settings.

11.2 Reference Database Configuration for MCNCC

When comparing MCNCC against a database of shoeprints, it yields a hit@100 of 0.0283 and mAP@K of 0.0008 on crime-scene shoeprints from val-FID. These metrics are notably lower compared to when using tread depths from the shoe database, where MCNCC achieves a hit@100 of 0.0849 and mAP@100 of 0.0018.

Table 9: Benchmarking on real crime-scene prints from val-FID, we assess the impact of simulated partial print masks. Using hit@100 and mAP@100 as metrics, we compare the performance of prior methods trained on our dataset with our data augmentation. The mAP@100 values reveal that prior methods tend to perform better when trained without masks simulating partial prints. *CriSp* consistently achieves superior performance on both metrics, regardless of the presence of masks.

method	w/o masks		w/ masks	
	hit@100	mAP@100	hit@100	mAP@100
IJCV'19 MCNCC [26]	0.0849	0.0018	-	-
NeurIPS'20 SupCon [25]	0.0755	0.0096	0.0849	0.0001
ICLR'21 FIRE [51]	0.2075	0.0398	0.0660	0.0030
CVPR'23 SketchLVM [42]	0.1981	0.0384	0.2547	0.0445
CVPR'23 ZSE-SBIR [31]	0.4528	0.1412	0.4623	0.1358
Ours	0.4528	0.1765	0.5472	0.2071

12 Evaluation Metric - Mean Average Precision at K

Mean average precision at K (mAP@K) considers both the number of positive matches and their positions in the ranking list. It rewards the system's ability to retrieve positive matches early. MAP@K is defined as follow:

$$\text{mAP@K} = \frac{1}{Q} \sum_{q=1}^Q AP@K_q \quad (2)$$

where $AP@K_q$ is the average precision at K for query q . $AP@K$ is calculated as follows:

$$AP@K_q = \frac{1}{N} \sum_{k=1}^K Precision@k \times rel(k) \quad (3)$$

where N is the total number of positive matches for a particular query. Since we are only interested in the top K retrievals, we limit N to an upper bound of K . $Precision(k)$ is the precision calculated at each position and is defined as $\frac{pos_k}{k}$ where pos_k represents the number of positive matches in the top k retrievals. The final term, $rel(k)$, equals 1 if the item at position k is a positive match and 0 otherwise.

13 Distribution of Shoe Models From Validation Sets in Reference Database

Table 6 provides insights into the distribution of ground-truth shoe models from our validation sets within the reference shoe database. Additionally, we present the count of distinct tread patterns that were either seen or unseen during training to facilitate comprehension. In Sec. 10.1, we assess the generalization performance of our model compared to state-of-the-art methods.

14 Data augmentation to Simulate Crime-Scene Shoeprints

Our data augmentation module *Aug* simulates noisy and occluded crime-scene shoeprints from clean, fully-visible shoeprints. It introduces three types of degradation: occlusion, erasure, and noise.

- For occlusion, we simulate overlapping prints and quadrilaterals. Overlapping prints mimic the common occurrence of multiple shoeprints overlapping at a crime scene. We achieve this by randomly rotating and translating the predicted print and overlaying it onto itself. Quadrilaterals, resembling papers, rulers, or other marks, are added to simulate typical occlusions found in crime-scene shoeprint images.
- Erasure is incorporated to mimic the grainy nature of prints left at crime scenes. This involves selectively removing parts of the predicted shoeprint using either a Gaussian or Perlin distribution. Gaussian distribution is a standard choice for data augmentation, while Perlin noise provides a more nuanced representation of noise variations found in real images.
- Noise is added to represent background clutter. Gaussian or Perlin noise is overlaid on the predicted prints to simulate the clutter typically present in crime-scene images.

These degradations are applied dynamically during training, with each being optional.

15 Implementation Details

We use a batch size of 4, where we randomly select 4 shoe models and then include two random instances per shoe model in each batch. During our experiments, training images of size 192 x 384 are encoded to a dimension of $H=6$ and $W = 12$. We use an Adam optimizer with a learning rate of 0.1 and set $\tau = 0.07$.